Belle II Preprint 2025-009
KEK Preprint 2025-7

Measurement of the time-integrated *CP* asymmetry in $D^0 \to \pi^0\pi^0$ decays at Belle II

I. Adachi, Y. Ahn, N. Akopov, S. Alghamdi, M. Alhakami, A. Aloisio, N. Althubiti, K. Amos, M. Angelsmark, N. Anh Ky, C. Antonioli, D. M. Asner, H. Atmacan, T. Aushev, M. Aversano, R. Ayad, V. Babu, H. Bae, N. K. Baghel, S. Bahinipati, P. Bambade, Sw. Banerjee, M. Barrett, M. Bartl, J. Baudot, A. Baur, A. Beaubien, F. Becherer, J. Becker, J. V. Bennett, F. U. Bernlochner, V. Bertacchi, M. Bertemes, E. Bertholet, M. Bessner, S. Bettarini, B. Bhuyan, F. Bianchi, T. Bilka, D. Biswas, A. Bobrov, D. Bodrov, A. Bondar, J. Borah, A. Boschetti, A. Bozek, M. Bračko, P. Branchini, R. A. Briere, T. E. Browder, A. Budano, S. Bussino, M. Campajola, L. Cao, G. Casarosa, C. Cecchi, P. Cheema, B. G. Cheon, K. Chilikin, J. Chin, K. Chirapatpimol, H.-E. Cho, K. Cho, S.-J. Cho, S.-K. Choi, S. Choudhury, I. Consigny, L. Corona, J. X. Cui, E. De La Cruz-Burelo, S. A. De La Motte, G. De Pietro, R. de Sangro, M. Destefanis, A. Di Canto, J. Dingfelder, Z. Doležal, I. Domínguez Jiménez, T. V. Dong, M. Dorigo, G. Dujany, P. Ecker, D. Epifanov, J. Eppelt, R. Farkas, P. Feichtinger, T. Ferber, T. Fillinger, C. Finck, G. Finocchiaro, A. Fodor, F. Forti, B. G. Fulsom, A. Gabrielli, A. Gale, E. Ganiev, M. Garcia-Hernandez, R. Garg, G. Gaudino, V. Gaur, V. Gautam, A. Gaz, A. Gellrich, D. Ghosh, H. Ghumaryan, G. Giakoustidis, R. Giordano, A. Giri, P. Gironella Gironell, B. Gobbo, R. Godang, O. Gogota, P. Goldenzweig, W. Gradl, E. Graziani, D. Greenwald, Z. Gruberová, K. Gudkova, I. Haide, Y. Han, H. Hayashii, S. Hazra, C. Hearty, M. T. Hedges, A. Heidelbach, G. Heine, I. Heredia de la Cruz, M. Hernández Villanueva, T. Higuchi, M. Hoek, M. Hohmann, P. Horak, C.-L. Hsu, T. Iijima, K. Inami, G. Inguglia, N. Ipsita, A. Ishikawa, R. Itoh, M. Iwasaki, P. Jackson, D. Jacobi, W. W. Jacobs, D. E. Jaffe, Q. P. Ji, S. Jia, Y. Jin, A. Johnson, J. Kandra, K. H. Kang, G. Karyan, T. Kawasaki, F. Keil, C. Ketter, M. Khan, C. Kiesling, D. Y. Kim, J.-Y. Kim, K.-H. Kim, K. Kinoshita, P. Kodyš, T. Koga, S. Kohani, K. Kojima, A. Korobov, S. Korpar, E. Kovalenko, R. Kowalewski, P. Križan, P. Krokovny, K. Kumara, T. Kunigo, A. Kuzmin, Y.-J. Kwon, K. Lalwani, T. Lam, J. S. Lange, T. S. Lau, M. Laurenza, R. Leboucher, F. R. Le Diberder, M. J. Lee, C. Lemettais, P. Leo, H.-J. Li, L. K. Li, Q. M. Li, W. Z. Li, Y. Li, Y. B. Li, Y. P. Liao, J. Libby, J. Lin, S. Lin, V. Lisovskyi, M. H. Liu, Q. Y. Liu, Y. Liu, Z. Liu, D. Liventsev, S. Longo, C. Lyu, Y. Ma, C. Madaan, M. Maggiora, S. P. Maharana, R. Maiti, G. Mancinelli, R. Manfredi, E. Manoni, M. Mantovano, D. Marcantonio, S. Marcello, C. Marinas, C. Martellini, A. Martens, T. Martinov, L. Massaccesi, M. Masuda, S. K. Maurya, M. Maushart, J. A. McKenna, F. Meier, D. Meleshko, M. Merola, C. Miller, M. Mirra, S. Mitra, K. Miyabayashi, R. Mizuk, G. B. Mohanty, S. Moneta, H.-G. Moser, M. Nakao, H. Nakazawa, Y. Nakazawa, M. Naruki, Z. Natkaniec, A. Natochii, M. Nayak, M. Neu, S. Nishida, S. Ogawa, R. Okubo, H. Ono, E. R. Oxford, G. Pakhlova, S. Pardi, K. Parham, H. Park, J. Park, K. Park, S.-H. Park, A. Passeri, S. Patra, R. Pestotnik, L. E. Piilonen, P. L. M. Podesta-Lerma, T. Podobnik, A. Prakash, C. Praz, S. Prell, E. Prencipe, M. T. Prim, S. Privalov, H. Purwar, P. Rados, G. Raeuber, S. Raiz, V. Raj, K. Ravindran, J. U. Rehman, M. Reif, S. Reiter, M. Remnev, L. Reuter, D. Ricalde Herrmann, I. Ripp-Baudot, G. Rizzo, J. M. Roney, A. Rostomyan, N. Rout, L. Salutari, D. A. Sanders, S. Sandilya, L. Santelj, V. Savinov, B. Scavino, C. Schmitt, J. Schmitz, S. Schneider, M. Schnepf, C. Schwanda, A. J. Schwartz, Y. Seino, A. Selce, K. Senyo, J. Serrano, M. E. Sevior, C. Sfienti, W. Shan, X. D. Shi, T. Shillington, J.-G. Shiu, D. Shtol, B. Shwartz, A. Sibidanov, F. Simon, J. Skorupa, R. J. Sobie, M. Sobotzik, A. Soffer, A. Sokolov, E. Solovieva, S. Spataro, B. Spruck, M. Starič, P. Stavroulakis, S. Stefkova, R. Stroili, Y. Sue,

M. Sumihama, N. Suwonjandee, H. Svidras, M. Takizawa, K. Tanida, F. Tenchini, F. Testa, O. Tittel, R. Tiwary, E. Torassa, K. Trabelsi, F. F. Trantou, I. Tsaklidis, M. Uchida, I. Ueda, T. Uglov, K. Unger, Y. Unno, K. Uno, S. Uno, Y. Ushiroda, R. van Tonder, K. E. Varvell, M. Veronesi, A. Vinokurova, V. S. Vismaya, L. Vitale, R. Volpe, A. Vossen, S. Wallner, M.-Z. Wang, A. Warburton, M. Watanabe, S. Watanuki, C. Wessel, E. Won, B. D. Yabsley, S. Yamada, W. Yan, S. B. Yang, J. Yelton, J. H. Yin, K. Yoshihara, J. Yuan, Y. Yusa, L. Zani, M. Zeyrek, B. Zhang, V. Zhilich, J. S. Zhou, Q. D. Zhou, L. Zhu, and R. Žlebčík
(The Belle II Collaboration)

We measure the time-integrated CP asymmetry, A_{CP}, in $D^0 \to \pi^0\pi^0$ decays reconstructed in $e^+e^- \to c\bar{c}$ events collected by Belle II during 2019–2022. The data corresponds to an integrated luminosity of 428 fb^{-1}. The D^0 decays are required to originate from the flavor-conserving $D^{*+} \to D^0\pi^+$ decay to determine the charm flavor at production time. Control samples of $D^0 \to K^-\pi^+$ decays, with or without an associated pion from a D^{*+} decay, are used to correct for detection asymmetries. The result, $A_{CP}(D^0 \to \pi^0\pi^0) = (0.30 \pm 0.72 \pm 0.20)\%$, where the first uncertainty is statistical and the second systematic, is consistent with CP symmetry.

PACS numbers:

I. INTRODUCTION

Searches for charge-parity (CP) violation in charm decays offer the opportunity to probe for physics beyond the standard model. Since, to a good approximation, the third generation of quarks can be ignored when describing charm transitions, CP-violation effects are expected to be tiny, with standard-model asymmetries typically ranging from 10^{-3} to 10^{-4} [1–5]. New dynamics may alter the expected decay or, for neutral mesons, flavor-mixing rates and introduce larger CP-violation effects. After decades of experimental efforts, CP violation in charm transitions has been observed only as the difference between the time-integrated CP asymmetries of $D^0 \to K^+K^-$ and $D^0 \to \pi^+\pi^-$ decays [6], with strong evidence that CP violation occurs mainly in the direct decay $D^0 \to \pi^+\pi^-$ [7]. (Throughout this paper, charge-conjugate modes are implied unless stated otherwise.) These results can be interpreted either as a sign of new dynamics or as an enhancement of the subleading amplitude mediated by non-perturbative QCD [8–18]. Moreover, they indicate a larger than expected breaking of the U-spin symmetry, which requires the CP asymmetries of the direct $D^0 \to K^+K^-$ and $D^0 \to \pi^+\pi^-$ decays to have equal magnitudes and opposite signs: $|A_{CP}^{\rm dir}(D^0 \to K^+K^-)| = -|A_{CP}^{\rm dir}(D^0 \to \pi^+\pi^-)|$ [19].

Precise measurements of CP asymmetries in the isospin-related $D^+ \to \pi^+\pi^0$ and $D^0 \to \pi^0\pi^0$ modes can help to clarify the picture [20, 21]. In the standard model, direct CP violation in Cabibbo-suppressed charm decays is generated by the interference of a leading tree-level amplitude and a suppressed $\Delta I = 1/2$ QCD-penguin amplitude, which changes isospin by half a unit. The $\pi^+\pi^0$ final state has isospin $I = 2$ and cannot be reached from the $I = 1/2$ initial state via a $\Delta I = 1/2$ transition. Hence, in the standard model, $A_{CP}^{\rm dir}(D^+ \to \pi^+\pi^0) = 0$. On the contrary, the $\pi^0\pi^0$ and $\pi^+\pi^-$ final states can have $I = 0$ or $I = 2$ and hence can have nonzero direct CP asymmetries in the standard model. As an example, recent experimental results imply that $A_{CP}^{\rm dir}(D^0 \to \pi^0\pi^0)$ may be as large as 1% [22]. The following sum-rule helps determine the source of CP violation: [20, 23]

$$R = \frac{A_{CP}^{\rm dir}(D^0 \to \pi^+\pi^-)}{1 + \frac{\tau_{D^0}}{\mathcal{B}_{+-}}\left(\frac{\mathcal{B}_{00}}{\tau_{D^0}} - \frac{2}{3}\frac{\mathcal{B}_{+0}}{\tau_{D^+}}\right)} + \frac{A_{CP}^{\rm dir}(D^0 \to \pi^0\pi^0)}{1 + \frac{\tau_{D^0}}{\mathcal{B}_{00}}\left(\frac{\mathcal{B}_{+-}}{\tau_{D^0}} - \frac{2}{3}\frac{\mathcal{B}_{+0}}{\tau_{D^+}}\right)} + \frac{A_{CP}^{\rm dir}(D^+ \to \pi^+\pi^0)}{1 - \frac{3}{2}\frac{\tau_{D^+}}{\mathcal{B}_{+0}}\left(\frac{\mathcal{B}_{00}}{\tau_{D^0}} + \frac{\mathcal{B}_{+-}}{\tau_{D^0}}\right)}, \quad (1)$$

where τ_{D^0} and τ_{D^+} are the lifetimes of D^0 and D^+ mesons, and, $\mathcal{B}_{+-}$, $\mathcal{B}_{00}$ and $\mathcal{B}_{+0}$ are the D meson branching fractions to $\pi^+\pi^-$, $\pi^0\pi^0$ and $\pi^+\pi^0$ decays. If R is measured to be nonzero, then CP violation arises from the $\Delta I = 1/2$ amplitude. If R is zero, and at least one of the direct CP asymmetries is nonzero, then CP violation arises from a beyond-standard-model $\Delta I = 3/2$ amplitude. The value is measured to be $R = (0.9 \pm 3.1) \times 10^{-3}$, where the uncertainty is dominated by the asymmetry of the $\pi^0\pi^0$ final state [23]. The most precise measurement of the time-integrated CP asymmetry in $D^0 \to \pi^0\pi^0$ available to date comes from the Belle collaboration, $(-0.03 \pm 0.64 \pm 0.10)\%$ [24], where the first uncertainty is statistical and the second systematic. (Indirect CP violation induced by D^0-$\overline{D}^0$ mixing is precisely measured in other channels [25] and subtracted from the time-integrated asymmetry when computing R [4, 26].) Belle II is the only existing experiment capable of improving this measurement and the determination of the sum rule.

In this paper, we report a measurement of the time-integrated CP asymmetry in $D^0 \to \pi^0\pi^0$ decays,

$$A_{CP}(D^0 \to \pi^0\pi^0) = \frac{\Gamma(D^0 \to \pi^0\pi^0) - \Gamma(\overline{D}^0 \to \pi^0\pi^0)}{\Gamma(D^0 \to \pi^0\pi^0) + \Gamma(\overline{D}^0 \to \pi^0\pi^0)} \quad (2)$$

where Γ is the decay-time integrated rate, which includes effects due to D^0-$\overline{D}^0$ mixing. The measurement uses

$e^+e^- \to c\bar{c}$ data collected by Belle II between 2019 and 2022, which correspond to an integrated luminosity of $428\,\mathrm{fb}^{-1}$. To determine the production flavor of the neutral D meson, we reconstruct $D^0 \to \pi^0\pi^0$ decays originating from $D^{*+} \to D^0\pi^+$ decays. We refer to D^0 mesons originating from identified D^{*+} decays as tagged decays, and to the low-momentum flavor-tagging pion as the "soft" pion or π_s. To measure the *CP* asymmetry, we determine the observed asymmetry between the number of detected decays of opposite flavor,

$$A^{\pi^0\pi^0} = \frac{N[D^{*+}\to(D^0\to\pi^0\pi^0)\pi^+]-N[D^{*-}\to(\bar{D}^0\to\pi^0\pi^0)\pi^-]}{N[D^{*+}\to(D^0\to\pi^0\pi^0)\pi^+]+N[D^{*-}\to(\bar{D}^0\to\pi^0\pi^0)\pi^-]}\,. \tag{3}$$

This raw asymmetry is a sum of contributions from *CP* violation, A_{CP}; from the forward-backward asymmetric production of D^{*+} mesons in $e^+e^- \to c\bar{c}$ events, $A_\mathrm{P}^{D^{*+}}$; and from charge asymmetries in the detection efficiency of positive and negative soft pions, $A_\epsilon^{\pi_\mathrm{s}}$:

$$A^{\pi^0\pi^0} = A_{CP}(D^0 \to \pi^0\pi^0) + A_\mathrm{P}^{D^{*+}} + A_\epsilon^{\pi_\mathrm{s}}\,. \tag{4}$$

We use high-yield control samples of tagged and untagged Cabibbo-favored $D^0 \to K^-\pi^+$ decays, where *CP* violation can be neglected, to correct for the instrumental asymmetries. The raw asymmetries of these decays are

$$A^{K\pi} = A_\mathrm{P}^{D^{*+}} + A_\epsilon^{\pi_\mathrm{s}} + A_\epsilon^{K\pi} \tag{5}$$

and

$$A^{K\pi,\mathrm{untag}} = A_\mathrm{P}^{D^0} + A_\epsilon^{K\pi}\,, \tag{6}$$

where $A_\epsilon^{K\pi}$ is the detection asymmetry of the $K^-\pi^+$ pair. In $e^+e^- \to c\bar{c}$ events, charmed mesons are produced with a forward-backward asymmetry due to γ-Z^0 interference and higher-order effects [27–29]. Since the acceptance of the Belle II detector is not the same in the forward and backward directions, a charge asymmetry in the production of charmed mesons remains. Being an odd function of the cosine of the charmed-meson polar angle in the e^+e^- center-of-mass system, $\cos\theta_\mathrm{cms}$, this production asymmetry is suppressed by averaging the raw asymmetries from forward and backward decays:

$$A'^{f} = \frac{A^f(\cos\theta_\mathrm{cms} < 0) + A^f(\cos\theta_\mathrm{cms} > 0)}{2}\,, \tag{7}$$

for $f = \pi^0\pi^0$; $K\pi$; $K\pi$, untag. Assuming that the detection asymmetries for different decays can be made identical by weighting the events, the *CP* asymmetry in $D^0 \to \pi^0\pi^0$ is then

$$A_{CP}(D^0 \to \pi^0\pi^0) = A'^{\pi^0\pi^0} - A'^{K\pi} + A'^{K\pi,\mathrm{untag}}\,, \tag{8}$$

where the difference between the first two terms cancels the soft-pion detection asymmetry, and the difference between the second and third terms cancels the $K^-\pi^+$ detection asymmetry. To avoid potential bias, the measured value of $A^{\pi^0\pi^0}$ remained unexamined until the entire analysis procedure was finalized and all uncertainties were determined.

The paper is organized as follows. Section II provides an overview of the Belle II detector and of the simulation samples used in the measurement. The reconstruction and selection of both the signal $D^0 \to \pi^0\pi^0$ and control $D^0 \to K^-\pi^+$ decays are presented in Section III. Section IV discusses the weighting of the control modes to match the kinematic distributions of the signal mode and ensure an accurate cancellation of the detector asymmetries. Determination of the raw asymmetries is covered in Section V, followed by a discussion of the systematic uncertainties affecting the measurement in Section VI. Final results are presented in Section VII, followed by concluding remarks.

II. BELLE II DETECTOR AND SIMULATION

The Belle II detector [30, 31] operates at the SuperKEKB asymmetric-energy e^+e^- collider [32]. It has a cylindrical geometry and consists of a silicon vertex detector comprising two inner layers of pixel detectors and four outer layers of double-sided strip detectors, a 56-layer central drift chamber, a time-of-propagation detector, an aerogel ring-imaging Cherenkov detector, and an electromagnetic calorimeter made of CsI(Tl) crystals, all located inside a 1.5 T superconducting solenoid. A flux return outside the solenoid is instrumented with resistive-plate chambers and plastic scintillator modules to detect muons and K_L^0 mesons. For the data used in this paper only part of the second layer of the pixel detector, covering 15% of the azimuthal angle, was installed. The z axis of the laboratory frame is defined as the central axis of the solenoid, with its positive direction determined by the direction of the electron beam.

We use simulated event samples to identify sources of background, optimize selection criteria, match the kinematic distributions of signal and control decays, determine fit models, and validate the analysis procedure. We generate $e^+e^- \to \Upsilon(4S)$ events and simulate particle decays with the EvtGen generator [33]; we generate continuum $e^+e^- \to q\bar{q}$ (where q is a u, d, c, or s quark) with KKMC [34] and Pythia8 [35]; we simulate final-state radiation with Photos [36, 37]; we simulate detector response using Geant4 [38]. Beam backgrounds are taken into account by overlaying random-trigger data. The data and simulation samples are processed using the Belle II analysis software framework [39, 40].

III. EVENT SELECTION

A. $D^0 \to \pi^0\pi^0$ signal sample

We reconstruct photon candidates from localized energy deposits, clusters, in the electromagnetic calorimeter that are consistent with an electromagnetic shower based on pulse-shape discrimination [41]. The clusters should have a polar angle in the laboratory frame, θ, within the acceptance of the drift chamber ($17 < \theta < 150^\circ$) to ensure that they are not matched to tracks. They must contain energy from at least two crystals and an energy deposit greater than 25 MeV if located in the forward ($12.4 < \theta < 31.4^\circ$) or barrel ($32.2 < \theta < 128.7^\circ$) regions, and greater than 40 MeV if in the backward region ($130.7 < \theta < 155.7^\circ$). Two photon candidates are then combined to form a neutral pion candidate if their mass is in $[105, 150]\,\mathrm{MeV}/c^2$ (the typical diphoton mass resolution is $7\,\mathrm{MeV}/c^2$). Pairs of π^0 candidates are combined to form $D^0 \to \pi^0\pi^0$ candidates and the dipion mass, $m(\pi^0\pi^0)$, is required to be in $[1.6,2.1]\,\mathrm{GeV}/c^2$.

Soft pion candidates are charged particles that are in the acceptance of the drift chamber and originate from the e^+e^- interaction region, meaning that they have longitudinal and transverse distances of closest approach to the e^+e^- interaction point smaller than 3 cm and 1 cm, respectively. A D^0 candidate and a soft pion candidate are then combined to form $D^{*+} \to D^0\pi^+$ candidates. The difference between the reconstructed D^{*+} and D^0 masses, Δm, must not exceed $160\,\mathrm{MeV}/c^2$. The D^{*+} candidates are subject to a fit that uses both kinematic and spatial information and constrains the D^{*+} vertex to the measured position of the beam interaction point [42]. Only candidates with successful fits and having χ^2 probabilities larger than 0.001 are retained for subsequent analysis. The momentum of the D^0 candidate in the e^+e^- center-of-mass system is required to exceed $2.5\,\mathrm{GeV}/c$ to suppress events where the D^0 candidate originates from the decay of a B meson, since D^0 mesons from this source may have a different production asymmetry.

We use a histogram-based gradient-boosting decision tree [43] (HBDT) to discriminate signal from background made of fake π^0 candidates and neutral pions originating from unrelated processes. The HBDT uses 14 input variables: the momentum of the D^0 candidate in the e^+e^- center-of-mass system, the momenta of the two π^0 candidates, the transverse momentum of the soft pion, the opening angle between the two photons of each π^0 decay, and for every photon in the reconstruction chain, the output of two multivariate classifiers that use shower-related variables to suppress energy clusters due to beam-related background or hadronic showers. The HBDT is trained and tested on independent samples of simulated decays to mitigate overtraining. To suppress background, the HBDT output is required to be larger than a threshold value that maximizes the figure-of-merit $N_{\rm sig}/\sqrt{N_{\rm sig}+N_{\rm bkg}}$, where $N_{\rm sig}$ and $N_{\rm bkg}$ are signal and background yields in the region defined by $m(\pi^0\pi^0) \in [1.78, 1.92]\,\mathrm{GeV}/c^2$ and $\Delta m \in [0.144, 0.147]\,\mathrm{GeV}/c^2$, as estimated using simulation. The HBDT requirement rejects 95% of the background while retaining 85% of the signal. After this selection, 9% of events have multiple D^{*+} candidates. In such cases, we retain the candidate with the highest HBDT output value. According to simulation, this criterion selects the correct candidate in 84% of cases.

B. $D^0 \to K^-\pi^+$ control samples

The reconstruction of the control mode starts by selecting events that are inconsistent with Bhabha scattering and have at least three tracks with transverse momentum larger than $0.2\,\mathrm{GeV}/c$ that originate from the e^+e^- interaction region.

Charged kaon and pion candidates are required to be in the acceptance of the drift chamber, to originate from the e^+e^- interaction region, and to be identified as kaons and pions, respectively. Particle identification is performed using information from all subdetector systems, except for the pixel detector [44]. The kaon and pion-identification efficiencies are above 83% and 93%, respectively, with corresponding pion-as-kaon and kaon-as-pion misidentification rates below 5% and 10%. A negatively charged kaon candidate and a positively charged pion candidate are combined to form $D^0 \to K^-\pi^+$ candidates with an invariant mass, $m(K^-\pi^+)$, in $[1.814, 1.914]\,\mathrm{GeV}/c^2$. A vertex-kinematic fit [42] requiring the D^0 candidate momentum to point back to the e^+e^- interaction region is performed, and only candidates with fit χ^2 probabilities in excess of 0.001 are retained. To suppress events where the D^0 candidate originates from the decay of a B meson, the momentum of the D^0 candidate in the e^+e^- center-of-mass system is required to exceed $2.5\,\mathrm{GeV}/c$. All candidates are retained in the $< 1\%$ of events where more than one D^0 candidate is reconstructed. These D^0 candidates form the untagged control sample.

The tagged control sample is obtained by combining D^0 and soft-pion candidates to form $D^{*+} \to D^0\pi_s^+$ candidate decays with Δm values in the range $[142.0, 148.8]\,\mathrm{MeV}/c^2$. The soft pions are selected with the same requirements as for the signal mode. We suppress $D^{*+} \to D^0\pi_s^+$ decays with a mis- or partially reconstructed D^0 candidate to a negligible level by tightening the $m(K^-\pi^+)$ range to $[1.854, 1.874]\,\mathrm{GeV}/c^2$. The D^{*+} candidates are subject to a vertex-kinematic fit which constrains the D^{*+} decay vertex to the measured position of the e^+e^- interaction region. Only candidates having fit χ^2 probabilities larger than 0.001 are retained. We retain all candidates in the less than 1% of the events where multiple D^{*+} candidates are reconstructed.

IV. KINEMATIC WEIGHTING

Because detection asymmetries depend on kinematic properties, the cancellation provided by Equation (8) is realized accurately only if the kinematic distributions across the three samples are the same. The small differences that are present are reduced using a two-step weighting procedure. In the first step, we ensure that the soft-pion detection asymmetry is accurately subtracted by matching the two-dimensional $\cos\theta(\pi_{\rm s})$, $p(\pi_{\rm s})$ distribution of the tagged control sample to that of the signal decays. In the second step, to precisely subtract the $K^-\pi^+$ detection asymmetry, we match the four-dimensional distribution of $\cos\theta(K)$, $p(K)$, $\cos\theta(\pi)$, $p(\pi)$ of the untagged sample to match that of the previously weighted tagged sample. The weighting steps are performed directly in two and four dimensions, so any correlations between kinematic variables are taken into account. The weights are determined on a per-candidate basis using background-subtracted signal and control decays in data with a tool that relies on boosted decision trees [45]. The background is subtracted using the *sPlot* method [46] and the same fit model as used for the determination of the asymmetries (Section V). The effect of the weighting procedure is shown in Figure 1. Small differences remain only at the borders of the distributions, and thus affect only a small subset of the three samples. Systematic uncertainties are assigned in Section VI due to the imperfections in the weighting procedure.

V. DETERMINATION OF THE RAW ASYMMETRIES

The raw asymmetries are determined using unbinned maximum-likelihood fits to D^0 and $\overline{D}^0$ candidates in data using observables that discriminate signal and control decays from background. The fits are performed independently for positive and negative $\cos\theta_{\rm cms}$. Using ensembles of pseudoexperiments generated from the assumed probability density functions (PDFs), the fits are shown to return unbiased determinations of the asymmetries and uncertainties with proper statistical coverage.

A. $D^0\to\pi^0\pi^0$ signal sample

In the signal sample, we use the two-dimensional $m(\pi^0\pi^0)$ *vs.* Δm distribution to discriminate among four components: signal $D^{*+}\to D^0(\to\pi^0\pi^0)\pi^+$ decays; background due to $D^{*+}\to D^0(\to K^0_{\rm S}\pi^0)\pi^+$ decays with $K^0_{\rm S}\to\pi^0\pi^0$, in which one π^0 meson from the $K^0_{\rm S}$ decay is not reconstructed; random-pion background from correctly reconstructed $D^0\to\pi^0\pi^0$ decays associated with unrelated $\pi_{\rm s}$ candidates; and combinatorial background due to unrelated combinations of final-state particles. Signal decays peak at the expected value of the D^0 mass in $m(\pi^0\pi^0)$ and of the D^{*+}-D^0 mass difference in Δm. Candidates $D^{*+}\to D^0(\to K^0_{\rm S}\pi^0)\pi^+$ decays have low $m(\pi^0\pi^0)$ because of the missing π^0, but still peak in Δm although with broader resolution than the signal. The random-pion background peaks like the signal in $m(\pi^0\pi^0)$ and does not peak in Δm. The combinatorial background does not peak in either $m(\pi^0\pi^0)$ or Δm.

The two-dimensional PDFs of signal, random-pion, and combinatorial background decays factorize into the product of two one-dimensional PDFs. The $m(\pi^0\pi^0)$ distribution of signal decays is modeled using the sum of a Johnson's S_U distribution [47],

$$J(x|\mu,\sigma,\delta,\gamma)\propto\frac{e^{-\frac{1}{2}\left[\gamma+\delta\sinh^{-1}\left(\frac{x-\mu}{\sigma}\right)\right]^2}}{\sqrt{1+\left(\frac{x-\mu}{\sigma}\right)^2}}\,, \qquad (9)$$

and a Gaussian function. The Δm distribution is parameterized using a sum of a Johnson's S_U and two Gaussian functions. The random-pion background shares the same $m(\pi^0\pi^0)$ PDF as the signal and has a Δm distribution modeled by $(\Delta m-m_{\pi^+})^{\frac{1}{2}}+\alpha(\Delta m-m_{\pi^+})^{\frac{3}{2}}+\beta(\Delta m-m_{\pi^+})^{\frac{5}{2}}$, with m_{π^+} being the known value of the charged-pion mass [48]. The combinatorial background shares the same Δm distribution used for random-pion decays and has $m(\pi^0\pi^0)$ modeled by a second-order polynomial.

In the $D^0\to K^0_{\rm S}\pi^0$ component, the width of the Δm distribution correlates with $m(\pi^0\pi^0)$, which we parametrize analytically as a second-order polynomial. The parameters of the polynomial are determined from simulation. The two-dimensional PDF is the product of the Δm PDF, conditional on the value of $m(\pi^0\pi^0)$, and of the $m(\pi^0\pi^0)$ PDF. The first term is parametrized as the sum of a Johnson's S_U function and a Gaussian function where the σ parameter of the former accounts for the aforementioned correlation. The second term is given by the sum of a Gaussian and an exponential function.

Omitting the fit parameters from the list of arguments to simplify the notation, the total PDF is

$$P(m,\Delta m|...)=\sum_i f^i(1+qA^i)P^i(m,\Delta m|...)\,, \qquad (10)$$

where $q=1(-1)$ for D^0 ($\overline{D}^0$) candidates, and f^i and A^i are the fraction and raw asymmetry of the component i (and one fraction is expressed in terms of the others for proper normalization of the PDF). When fitting to the data, 18 parameters are floated: the component fractions and asymmetries, the μ and γ parameters of the Johnson's S_U function of the signal $m(\pi^0\pi^0)$ and Δm PDFs, the mean of the Gaussian function of the signal $m(\pi^0\pi^0)$ PDF, the μ and σ of the Johnson's S_U function of the $D^0\to K^0_{\rm S}\pi^0$ Δm PDF, the shape parameters of the combinatorial-background PDFs in $m(\pi^0\pi^0)$ and Δm. The remaining 21 shape parameters are fixed to the values obtained when fitting to simulated data.

Figure 2 shows the $m(\pi^0\pi^0)$ and Δm distributions of the data split in the positive and negative $\cos\theta_{\rm cms}$, with fit projection overlaid. In this fit, the random-pion component is neglected because its fraction is found to be

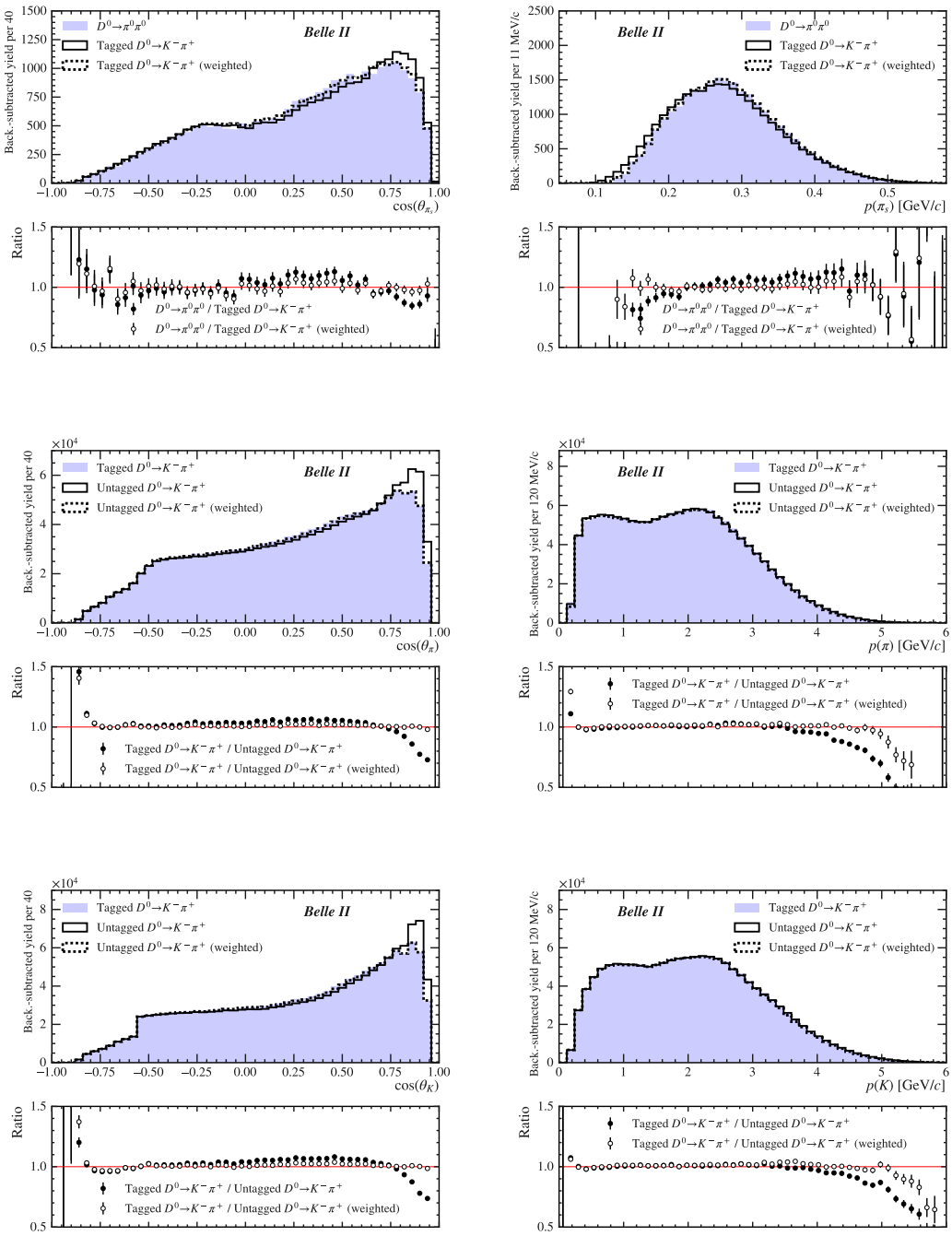

Figure 1: Distributions of $\cos\theta(\pi_s)$ and $p(\pi_s)$ of background-subtracted signal and tagged control decays (first row) ; $\cos\theta(\pi)$, $p(\pi)$, $\cos\theta(K)$, $p(K)$ of background-subtracted tagged and untagged control decays (second and third row); and the ratios before and after the kinematic weighting.

consistent with zero (removing two floating parameters from the fit). The fit model describes the data well and the signal yields are measured to be $14\,100 \pm 130$ and $11\,550 \pm 110$ in the forward and backward bins, respectively. The corresponding raw asymmetries are $(-2.20 \pm 0.95)\%$ and $(5.66 \pm 1.05)\%$. When averaged we obtain

$$A'^{\pi^0\pi^0} = (1.73 \pm 0.71)\% \,. \tag{11}$$

The uncertainties are statistical only.

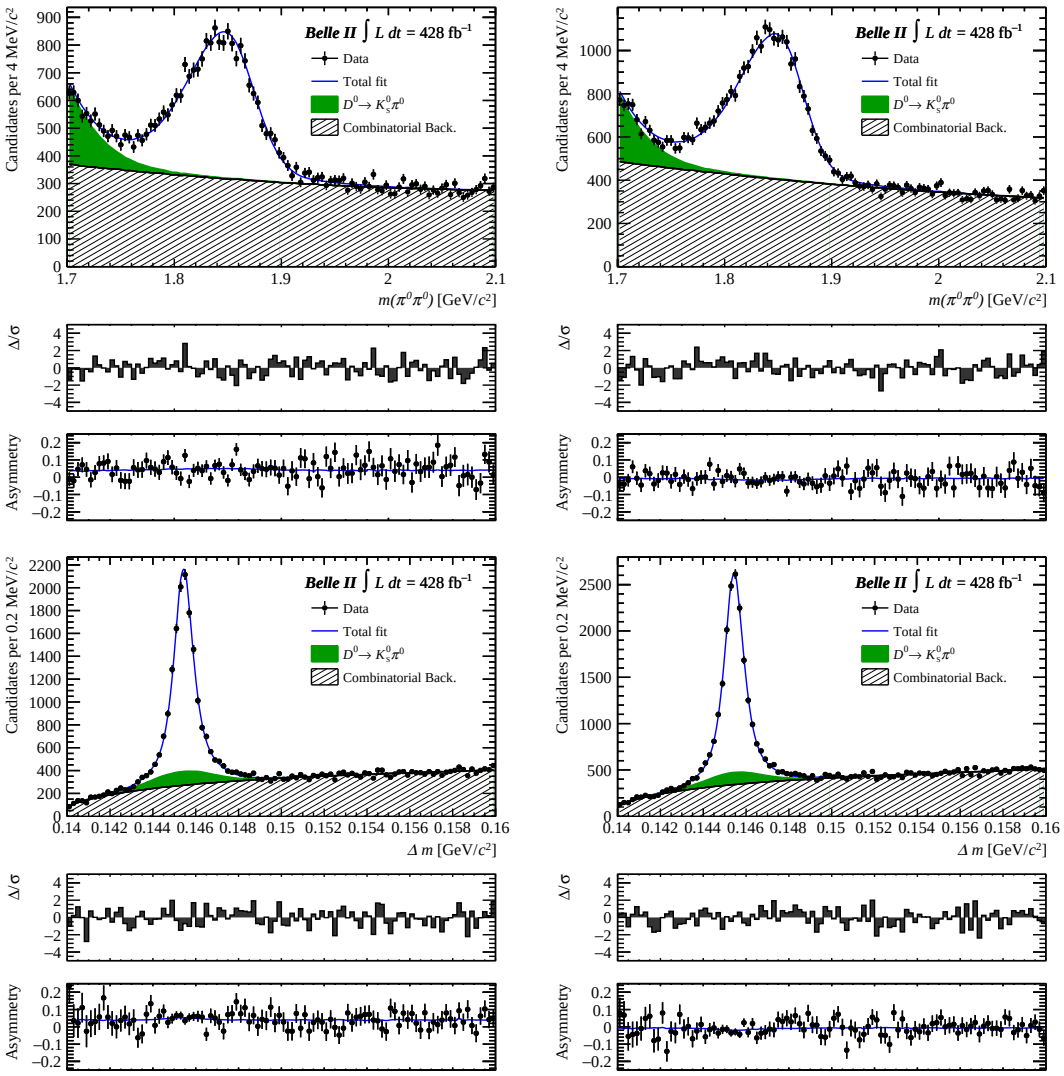

Figure 2: Distributions of $m(\pi^0\pi^0)$ (top) and Δm (bottom) for $D^0 \to \pi^0\pi^0$ candidates with $\cos\theta_{\rm cms}(D^{*+}) < 0$ (left) and $\cos\theta_{\rm cms}(D^{*+}) > 0$ (right), with fit projections overlaid. The middle panel of each plot shows the distribution of the difference between observed and fit values divided by the uncertainty (pull), the bottom panel shows the asymmetry between D^0 and $\overline{D}^0$ candidates with the fit projection overlaid.

B. $D^0 \to K^-\pi^+$ control samples

The raw asymmetry of the tagged control sample is determined from a fit to the Δm distribution, in which only two components are considered: the $D^{*+} \to D^0(\to K^-\pi^+)\pi^+$ decays, and a background made of both random-pion and combinatorial candidates. The Δm PDF of $D^0 \to K^-\pi^+$ decays is the sum of a Johnson's S_U and a Gaussian function, with common location and width parameters that are determined independently for D^0 and $\overline{D}^0$ decays to account for flavor-dependent mass biases and resolutions. The background component is modeled as $(\Delta m - m_{\pi^+})^\beta e^{-\lambda(\Delta m - m_{\pi^+})}$. The relative fractions of the components, their asymmetries and all shape parameters are floated in the fit (for a total of 14 floating parameters). Figure 3 shows the results of the fits to the data. The measured yields of $D^{*+} \to D^0(\to K^-\pi^+)\pi^+$ decays in the forward and backward bins are $796\,000 \pm 1\,200$ and $633\,700 \pm 1\,200$, respectively. The corresponding asymmetries, $(-0.86 \pm 0.13)\%$ and $(5.83 \pm 0.13)\%$, are averaged to obtain

$$A'^{K\pi} = (2.49 \pm 0.09)\%\,, \qquad (12)$$

where the uncertainties are statistical only.

For untagged decays, we fit to the $m(K^-\pi^+)$ distribution, again considering only two components. The untagged $D^0 \to K^-\pi^+$ decays are modeled using the sum of a Johnson S_U and a Gaussian function, with common mean and flavor-dependent width parameters. A straight line is used to model the $m(K^-\pi^+)$ distribution of the background with a flavor-dependent coeffi-

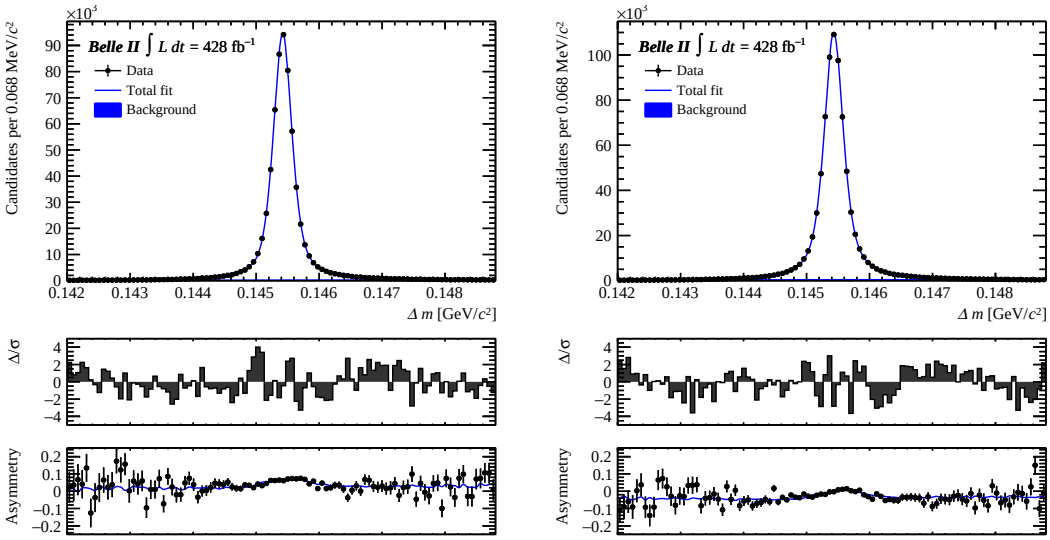

Figure 3: Distributions of Δm for tagged $D^0 \to K^-\pi^+$ candidates with $\cos\theta_{\rm cms}(D^*) < 0$ (left) and $\cos\theta_{\rm cms}(D^*) > 0$ (right), with fit projections overlaid. The middle panel of each plot shows the distribution of the difference between observed and fit values divided by the uncertainty (pull), the bottom panel shows the asymmetry between D^0 and $\overline{D}^0$ candidates with the fit projection overlaid.

cient. Also in this case, all parameters are determined from the fit. The results of the fit are shown in Figure 4. We measure $4\,294\,700 \pm 5\,600$ and $3\,374\,100 \pm 6\,500$ untagged $D^0 \to K^-\pi^+$ decays in the forward and backward bins, respectively. The corresponding asymmetries, $(-1.65 \pm 0.09)\%$ and $(3.75 \pm 0.11)\%$, are averaged to obtain

$$A'^{K\pi,\rm untag} = (1.05 \pm 0.07)\%\,, \qquad (13)$$

where the uncertainties are statistical only.

The raw-asymmetry values are consistent with expected differences in reconstruction asymmetries for charged particles in forward and backward directions. While the variation of the asymmetry as a function of mass is fairly well described by the fit model for $D^0 \to K^-\pi^+$ control samples (Figure 4, bottom panel), the *CP*-averaged distributions are not (Figure 4, middle panel). Systematic uncertainties are assigned in Section VI to cover the impact of the mismodeling on the measured asymmetries.

Using Equation (8), we determine the time-integrated *CP* asymmetry in $D^0 \to \pi^0\pi^0$ decays to be $(0.30 \pm 0.72)\%$, where the uncertainty is statistical only.

VI. SYSTEMATIC UNCERTAINTIES

The measurement is affected by the following main sources of systematic uncertainties: PDF modeling in the signal and control-sample fits, and kinematic weighting of control and signal samples. Other effects, such as those due to finite $\cos\theta_{\rm cms}$ resolution and nonuniform efficiency variation as a function of $|\cos\theta_{\rm cms}|$, are also investigated and found to be negligible. A summary of the estimated uncertainties is reported in Table I together with the sum in quadrature of all contributions.

Table I: Summary of uncertainties affecting the measurement of $A_{CP}(D^0 \to \pi^0\pi^0)$. The statistical uncertainty includes contributions from the signal and the control modes.

Source	Uncertainty (%)
Modeling in the $D^0 \to \pi^0\pi^0$ fit	0.15
Modeling in the tagged $D^0 \to K^-\pi^+$ fit	0.05
Modeling in the untagged $D^0 \to K^-\pi^+$ fit	0.09
Kinematic weighting	0.09
Total systematic	0.20
Statistical	0.72

We estimate the systematic uncertainties due to PDF modeling in the $D^0 \to \pi^0\pi^0$, tagged $D^0 \to K^-\pi$, and untagged $D^0 \to K^-\pi^+$ fits using simulation. From simulation we bootstrap (i.e., sampling with replacement) subsamples of the same size as the data, perform the fit, and compute the bias on the raw asymmetry as the average deviation from the true asymmetry of the full simulation sample. Fits to the simulated decays have similar qualities as observed in data. To cover possible data-simulation differences in detection and/or production asymmetries, the study is performed with input raw asymmetries for signal and control decays that span the range $[-2, 7]\%$. This range includes asymmetries that are either half or double the nominal asymmetry generated by the simulation. The root-mean-squared values of the biases from the ensemble of bootstrap samples are assigned as systematic uncertainties due to the imperfect modeling. The default fit models assume that most

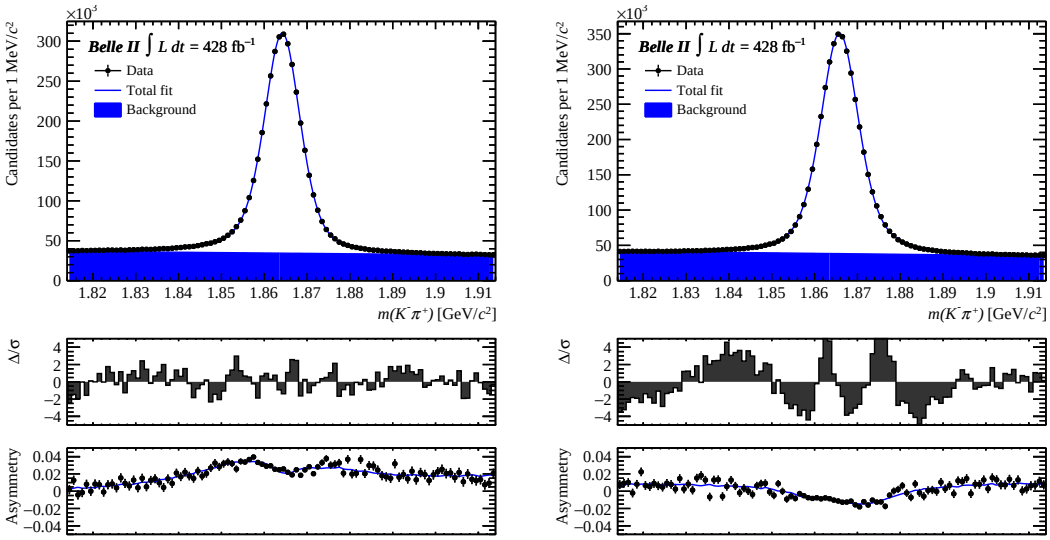

Figure 4: Distributions of $m(K^-\pi^+)$ for untagged $D^0 \to K^-\pi^+$ candidates with $\cos\theta_{\rm cms}(D^0) < 0$ (left) and $\cos\theta_{\rm cms}(D^0) > 0$ (right) in data, with fit projections overlaid. The middle panel of each plot shows the distribution of the difference between observed and fit values divided by the uncertainty (pull), the bottom panel shows the asymmetry between D^0 and $\overline{D}^0$ candidates with the fit projection overlaid.

shape parameters are flavor-independent. To verify this assumption, we refit the data replacing individual shape parameters with flavor-dependent ones. In all cases, the parameter asymmetries are consistent with zero and statistically insignificant shifts are observed in the measured A_{CP} values. The default $D^0 \to \pi^0\pi^0$ model includes 37 parameters, where 16 are left floating and the remaining 21 are fixed to the values obtained from simulation. The robustness of this setup is checked by varying the fixed parameters within their uncertainties. The impact on $A'^{\pi^0\pi^0}$ is found to be negligible compared to other uncertainties.

We estimate the systematic uncertainty due to the kinematic weighting by considering two sources of uncertainty: the accuracy of the background-subtraction procedure to obtain the kinematic distributions of the signal and control decays, and the choice of the variables used in the weighting procedure. For background subtraction, we rely on the *sPlot* method. Simulation shows that this approach could introduce an absolute shift in the estimated *CP* asymmetry of 0.05%. To test how the choice of kinematic variables impacts the result, we develop an alternative weighting procedure by replacing the momenta of the soft pion, kaon, and pion with their transverse momenta. The shift in A_{CP} observed when using the alternative weights is 0.07%. The sum in quadrature of the two shifts is assigned as systematic uncertainty due to the weighting procedure.

VII. FINAL RESULTS AND CONCLUSIONS

Using D^{*+}-tagged $D^0 \to \pi^0\pi^0$ decays reconstructed in the data sample collected by Belle II between 2019 and 2022, which corresponds to 428 fb^{-1} of integrated luminosity, we measure the time-integrated *CP* asymmetry in $D^0 \to \pi^0\pi^0$ decays to be

$$A_{CP}(D^0 \to \pi^0\pi^0) = (0.30 \pm 0.72 \pm 0.20)\%\,, \qquad (14)$$

where the first uncertainty is statistical and the second systematic. The result is consistent with *CP* symmetry and with the best existing measurement, from Belle [24]. It is 15% less precise than the Belle measurement, but it is based on a data sample less than one-half the size. The improved precision per luminosity is achieved through an improved event selection, which exploits Belle II's superior capabilities in the reconstruction of neutral pions.

We compute the isospin sum-rule of Equation (1) using our result, LHCb's measurement of $A_{CP}^{\rm dir}(D^0 \to \pi^+\pi^-)$ [7], the world-average value of $A_{CP}^{\rm dir}(D^+ \to \pi^+\pi^0)$ [23], Belle's measurement of $A_{CP}(D^0 \to \pi^0\pi^0)$ [24], LHCb's measurement of the indirect *CP*-violation parameter ΔY [25], the world-average values of the $D \to \pi\pi$ branching fractions [48], and the world-average values of the D^0 and D^+ lifetimes [48]. The direct *CP* asymmetry in $D^0 \to \pi^0\pi^0$ is obtained by subtracting ΔY from the time-integrated asymmetry assuming universality [4], and that the average decay time of the selected $D^0 \to \pi^0\pi^0$ decays is equal to the D^0 lifetime [26]. All inputs are assumed to be uncorrelated. We obtain $R = (1.5 \pm 2.5) \times 10^{-3}$, which shows that our measurement of $A_{CP}(D^0 \to \pi^0\pi^0)$ improves the precision of the sum rule by approximately 20% compared to the

current determination [23]. The sum rule is still limited by the precision on $A_{CP}(D^0 \to \pi^0\pi^0)$, so future measurements based on the larger samples being collected at Belle II will be critical to further constrain its value.

This work, based on data collected using the Belle II detector, which was built and commissioned prior to March 2019, was supported by Higher Education and Science Committee of the Republic of Armenia Grant No. 23LCG-1C011; Australian Research Council and Research Grants No. DP200101792, No. DP210101900, No. DP210102831, No. DE220100462, No. LE210100098, and No. LE230100085; Austrian Federal Ministry of Education, Science and Research, Austrian Science Fund (FWF) Grants DOI: 10.55776/P34529, DOI: 10.55776/J4731, DOI: 10.55776/J4625, DOI: 10.55776/M3153, and DOI: 10.55776/PAT1836324, and Horizon 2020 ERC Starting Grant No. 947006 "InterLeptons"; Natural Sciences and Engineering Research Council of Canada, Compute Canada and CANARIE; National Key R&D Program of China under Contract No. 2024YFA1610503, and No. 2024YFA1610504 National Natural Science Foundation of China and Research Grants No. 11575017, No. 11761141009, No. 11705209, No. 11975076, No. 12135005, No. 12150004, No. 12161141008, No. 12475093, and No. 12175041, and Shandong Provincial Natural Science Foundation Project ZR2022JQ02; the Czech Science Foundation Grant No. 22-18469S and Charles University Grant Agency project No. 246122; European Research Council, Seventh Framework PIEF-GA-2013-622527, Horizon 2020 ERC-Advanced Grants No. 267104 and No. 884719, Horizon 2020 ERC-Consolidator Grant No. 819127, Horizon 2020 Marie Sklodowska-Curie Grant Agreement No. 700525 "NIOBE" and No. 101026516, and Horizon 2020 Marie Sklodowska-Curie RISE project JENNIFER2 Grant Agreement No. 822070 (European grants); L'Institut National de Physique Nucléaire et de Physique des Particules (IN2P3) du CNRS and L'Agence Nationale de la Recherche (ANR) under Grant No. ANR-21-CE31-0009 (France); BMBF, DFG, HGF, MPG, and AvH Foundation (Germany); Department of Atomic Energy under Project Identification No. RTI 4002, Department of Science and Technology, and UPES SEED funding programs No. UPES/R&D-SEED-INFRA/17052023/01 and No. UPES/R&D-SOE/20062022/06 (India); Israel Science Foundation Grant No. 2476/17, U.S.-Israel Binational Science Foundation Grant No. 2016113, and Israel Ministry of Science Grant No. 3-16543; Istituto Nazionale di Fisica Nucleare and the Research Grants BELLE2, and the ICSC – Centro Nazionale di Ricerca in High Performance Computing, Big Data and Quantum Computing, funded by European Union – NextGenerationEU; Japan Society for the Promotion of Science, Grant-in-Aid for Scientific Research Grants No. 16H03968, No. 16H03993, No. 16H06492, No. 16K05323, No. 17H01133, No. 17H05405, No. 18K03621, No. 18H03710, No. 18H05226, No. 19H00682, No. 20H05850, No. 20H05858, No. 22H00144, No. 22K14056, No. 22K21347, No. 23H05433, No. 26220706, and No. 26400255, and the Ministry of Education, Culture, Sports, Science, and Technology (MEXT) of Japan; National Research Foundation (NRF) of Korea Grants No. 2016R1-D1A1B-02012900, No. 2018R1-A6A1A-06024970, No. 2021R1-A6A1A-03043957, No. 2021R1-F1A-1060423, No. 2021R1-F1A-1064008, No. 2022R1-A2C-1003993, No. 2022R1-A2C-1092335, No. RS-2023-00208693, No. RS-2024-00354342 and No. RS-2022-00197659, Radiation Science Research Institute, Foreign Large-Size Research Facility Application Supporting project, the Global Science Experimental Data Hub Center, the Korea Institute of Science and Technology Information (K24L2M1C4) and KREONET/GLORIAD; Universiti Malaya RU grant, Akademi Sains Malaysia, and Ministry of Education Malaysia; Frontiers of Science Program Contracts No. FOINS-296, No. CB-221329, No. CB-236394, No. CB-254409, and No. CB-180023, and SEP-CINVESTAV Research Grant No. 237 (Mexico); the Polish Ministry of Science and Higher Education and the National Science Center; the Ministry of Science and Higher Education of the Russian Federation and the HSE University Basic Research Program, Moscow; University of Tabuk Research Grants No. S-0256-1438 and No. S-0280-1439 (Saudi Arabia), and Researchers Supporting Project number (RSPD2025R873), King Saud University, Riyadh, Saudi Arabia; Slovenian Research Agency and Research Grants No. J1-50010 and No. P1-0135; Ikerbasque, Basque Foundation for Science, State Agency for Research of the Spanish Ministry of Science and Innovation through Grant No. PID2022-136510NB-C33, Spain, Agencia Estatal de Investigacion, Spain Grant No. RYC2020-029875-I and Generalitat Valenciana, Spain Grant No. CIDEGENT/2018/020; The Knut and Alice Wallenberg Foundation (Sweden), Contracts No. 2021.0174 and No. 2021.0299; National Science and Technology Council, and Ministry of Education (Taiwan); Thailand Center of Excellence in Physics; TUBITAK ULAKBIM (Turkey); National Research Foundation of Ukraine, Project No. 2020.02/0257, and Ministry of Education and Science of Ukraine; the U.S. National Science Foundation and Research Grants No. PHY-1913789 and No. PHY-2111604, and the U.S. Department of Energy and Research Awards No. DE-AC06-76RLO1830, No. DE-SC0007983, No. DE-SC0009824, No. DE-SC0009973, No. DE-SC0010007, No. DE-SC0010073, No. DE-SC0010118, No. DE-SC0010504, No. DE-SC0011784, No. DE-SC0012704, No. DE-SC0019230, No. DE-SC0021274, No. DE-SC0021616, No. DE-SC0022350, No. DE-SC0023470; and the Vietnam Academy of Science and Technology (VAST) under Grants No. NVCC.05.12/22-23 and No. DL0000.02/24-25.

These acknowledgements are not to be interpreted as an endorsement of any statement made by any of our

institutes, funding agencies, governments, or their representatives.

We thank the SuperKEKB team for delivering high-luminosity collisions; the KEK cryogenics group for the efficient operation of the detector solenoid magnet and IBBelle on site; the KEK Computer Research Center for on-site computing support; the NII for SINET6 network support; and the raw-data centers hosted by BNL, DESY, GridKa, IN2P3, INFN, and the University of Victoria.

[1] M. Golden and B. Grinstein, *Enhanced CP violations in hadronic charm decays*, Phys. Lett. B **222** (1989) 501.

[2] F. Buccella *et al.*, *Nonleptonic weak decays of charmed mesons*, Phys. Rev. D **51** (1995) 3478, arXiv:hep-ph/9411286.

[3] S. Bianco, F. L. Fabbri, D. Benson, and I. Bigi, *A Cicerone for the physics of charm*, Riv. Nuovo Cim. **26N7** (2003) 1, arXiv:hep-ex/0309021.

[4] Y. Grossman, A. L. Kagan, and Y. Nir, *New physics and CP violation in singly Cabibbo suppressed D decays*, Phys. Rev. D **75** (2007) 036008, arXiv:hep-ph/0609178.

[5] M. Artuso, B. Meadows, and A. A. Petrov, *Charm meson decays*, Ann. Rev. Nucl. Part. Sci. **58** (2008) 249, arXiv:0802.2934.

[6] LHCb collaboration, R. Aaij *et al.*, *Observation of CP violation in charm decays*, Phys. Rev. Lett. **122** (2019) 211803, arXiv:1903.08726.

[7] LHCb collaboration, R. Aaij *et al.*, *Measurement of the time-integrated CP asymmetry in $D^0 \to K^+K^-$ decays*, Phys. Rev. Lett. **131** (2023) 091802, arXiv:2209.03179.

[8] M. Chala, A. Lenz, A. V. Rusov, and J. Scholtz, *ΔA_{CP} within the Standard Model and beyond*, JHEP **07** (2019) 161, arXiv:1903.10490.

[9] A. Dery and Y. Nir, *Implications of the LHCb discovery of CP violation in charm decays*, JHEP **12** (2019) 104, arXiv:1909.11242.

[10] L. Calibbi, T. Li, Y. Li, and B. Zhu, *Simple model for large CP violation in charm decays, B-physics anomalies, muon $g-2$ and dark matter*, JHEP **10** (2020) 070, arXiv:1912.02676.

[11] Y. Grossman and S. Schacht, *The emergence of the $\Delta U = 0$ rule in charm physics*, JHEP **07** (2019) 020, arXiv:1903.10952.

[12] H.-Y. Cheng and C.-W. Chiang, *Revisiting CP violation in $D \to PP$ and VP decays*, Phys. Rev. D **100** (2019) 093002, arXiv:1909.03063.

[13] A. J. Buras, P. Colangelo, F. De Fazio, and F. Loparco, *The charm of 331*, JHEP **10** (2021) 021, arXiv:2107.10866.

[14] S. Schacht and A. Soni, *Enhancement of charm CP violation due to nearby resonances*, Phys. Lett. B **825** (2022) 136855, arXiv:2110.07619.

[15] I. Bediaga, T. Frederico, and P. C. Magalhães, *Enhanced Charm CP Asymmetries from Final State Interactions*, Phys. Rev. Lett. **131** (2023) 051802, arXiv:2203.04056.

[16] A. Pich, E. Solomonidi, and L. Vale Silva, *Final-state interactions in the CP asymmetries of charm-meson two-body decays*, Phys. Rev. D **108** (2023) 036026, arXiv:2305.11951.

[17] M. Gavrilova, Y. Grossman, and S. Schacht, *Determination of the $D \to \pi\pi$ ratio of penguin over tree diagrams*, Phys. Rev. D **109** (2024) 033011, arXiv:2312.10140.

[18] A. Lenz, M. L. Piscopo, and A. V. Rusov, *Two body non-leptonic D^0 decays from LCSR and implications for Δa_{CP}^{dir}*, JHEP **03** (2024) 151, arXiv:2312.13245.

[19] S. Schacht, *A U-spin anomaly in charm CP violation*, JHEP **03** (2023) 205, arXiv:2207.08539.

[20] Y. Grossman, A. L. Kagan, and J. Zupan, *Testing for new physics in singly Cabibbo suppressed D decays*, Phys. Rev. D **85** (2012) 114036, arXiv:1204.3557.

[21] A. J. Bevan and B. T. Meadows, *Bounding hadronic uncertainties in $c \to u$ decays*, Phys. Rev. D **90** (2014) 094028, arXiv:1310.0050.

[22] D. Wang, *Evidence of $A_{CP}(D^0 \to \pi^+\pi^-)$ implies observable CP violation in the $D^0 \to \pi^0\pi^0$ decay*, Eur. Phys. J. C **83** (2023) 279, arXiv:2207.11053.

[23] HFLAV group, Y. S. Amhis *et al.*, *Averages of b-hadron, c-hadron, and τ-lepton properties as of 2021*, Phys. Rev. D **107** (2023) 052008, arXiv:2206.07501, updated results and plots available at https://hflav.web.cern.ch/.

[24] Belle collaboration, N. K. Nisar *et al.*, *Search for CP violation in $D^0 \to \pi^0\pi^0$ decays*, Phys. Rev. Lett. **112** (2014) 211601, arXiv:1404.1266.

[25] LHCb collaboration, R. Aaij *et al.*, *Search for time-dependent CP violation in $D^0 \to K^+K^-$ and $D^0 \to \pi^+\pi^-$ decays*, Phys. Rev. D **104** (2021) 072010, arXiv:2105.09889.

[26] CDF collaboration, T. Aaltonen *et al.*, *Measurement of CP-violating asymmetries in $D^0 \to \pi^+\pi^-$ and $D^0 \to K^+K^-$ decays at CDF*, Phys. Rev. D **85** (2012) 012009, arXiv:1111.5023.

[27] F. A. Berends, K. J. F. Gaemers, and R. Gastmans, *α^3 contribution to the angular asymmetry in $e^+e^- \to \mu^+\mu^-$*, Nucl. Phys. B **63** (1973) 381.

[28] R. W. Brown, K. O. Mikaelian, V. K. Cung, and E. A. Paschos, *Electromagnetic background in the search for neutral weak currents via $e^+e^- \to \mu^+\mu^-$*, Phys. Lett. B **43** (1973) 403.

[29] R. J. Cashmore, C. M. Hawkes, B. W. Lynn, and R. G. Stuart, *The forward-backward asymmetry in $e^+e^- \to \mu^+\mu^-$ comparisons between the theoretical calculations at the one loop level in the Standard Model and with the experimental measurements*, Z. Phys. C **30** (1986) 125.

[30] Belle II collaboration, T. Abe *et al.*, *Belle II Technical Design Report*, arXiv:1011.0352.

[31] W. Altmannshofer *et al.*, *The Belle II physics book*, PTEP **2019** (2019) 123C01, Erratum ibid. **2020** (2020) 029201, arXiv:1808.10567.

[32] K. Akai, K. Furukawa, and H. Koiso, *SuperKEKB collider*, Nucl. Instrum. Meth. A **907** (2018) 188, arXiv:1809.01958.

[33] D. J. Lange, *The EvtGen particle decay simulation package*, Nucl. Instrum. Meth. A **462** (2001) 152.

[34] S. Jadach, B. F. L. Ward, and Z. Wąs, *The precision*

Monte Carlo event generator KK for two-fermion final states in e^+e^- collisions, Comput. Phys. Commun. **130** (2000) 260, arXiv:hep-ph/9912214.

[35] T. Sjöstrand *et al.*, *An Introduction to PYTHIA 8.2*, Comput. Phys. Commun. **191** (2015) 159, arXiv:1410.3012.

[36] E. Barberio, B. van Eijk, and Z. Wąs, *PHOTOS: A universal Monte Carlo for QED radiative corrections in decays*, Comput. Phys. Commun. **66** (1991) 115.

[37] E. Barberio and Z. Wąs, *PHOTOS: A Universal Monte Carlo for QED radiative corrections. Version 2.0*, Comput. Phys. Commun. **79** (1994) 291.

[38] GEANT4 collaboration, S. Agostinelli *et al.*, *GEANT4: A simulation toolkit*, Nucl. Instrum. Meth. **A506** (2003) 250.

[39] Belle II Framework Software Group, T. Kuhr *et al.*, *The Belle II Core Software*, Comput. Softw. Big Sci. **3** (2019) 1, arXiv:1809.04299.

[40] Belle II collaboration, *Belle II Analysis Software Framework (basf2)*, https://doi.org/10.5281/zenodo.5574115.

[41] S. Longo *et al.*, *CsI(Tl) pulse shape discrimination with the Belle II electromagnetic calorimeter as a novel method to improve particle identification at electron-positron colliders*, Nucl. Instrum. Meth. A **982** (2020) 164562, arXiv:2007.09642.

[42] Belle II Analysis Software Group, J.-F. Krohn *et al.*, *Global decay chain vertex fitting at Belle II*, Nucl. Instrum. Meth. A **976** (2020) 164269, arXiv:1901.11198.

[43] F. Pedregosa *et al.*, *Scikit-learn: Machine learning in Python*, J. Mach. Learn. Res. **12** (2011) 2825, arXiv:1201.0490.

[44] Belle II collaboration, I. Adachi *et al.*, *Charged-hadron identification at Belle II*, arXiv:2506.04355.

[45] A. Rogozhnikov, *Reweighting with Boosted Decision Trees*, J. Phys. Conf. Ser. **762** (2016) 012036, arXiv:1608.05806.

[46] M. Pivk and F. R. Le Diberder, *sPlot: A statistical tool to unfold data distributions*, Nucl. Instrum. Meth. A **555** (2005) 356, arXiv:physics/0402083.

[47] N. L. Johnson, *Systems of frequency curves generated by methods of translation*, Biometrika **36** (1949) 149.

[48] Particle Data Group, S. Navas *et al.*, *Review of particle physics*, Phys. Rev. D **110** (2024) 030001.